Additive Manufacturing Letters 3 (2022) 100052

Contents lists available at ScienceDirect

Additive Manufacturing Letters

journal homepage: www.elsevier.com/locate/addlet

Bulk-like ductility of cold spray additively manufactured copper in the as-sprayed state

Reeti Singh[a,*], Jan Kondás[a], Christian Bauer[a], Jan Cizek[b], Jan Medricky[b], Stefan Csaki[b], Jan Čupera[c], Radek Procházka[d], Daniel Melzer[d], Pavel Konopík[d]

[a] Impact Innovations GmbH, Bürgermeister-Steinberger-Ring 1, 84431 Haun/Rattenkirchen, Germany
[b] Institute of Plasma Physics of the Czech Academy of Sciences, Department of Materials Engineering, Za Slovankou 1782/3, 182 00 Prague 8, Czechia
[c] Brno University of Technology, Brno, Czech Republic Czech Academy of Sciences, Prague, Czechia
[d] COMTES FHT a.s., Průmyslová 995, 334 41 Dobřany, Czechia

ARTICLE INFO

Keywords:
Cold spray
Copper
High ductility
Additive manufacturing

ABSTRACT

In recent years, cold spray process is increasingly used for additive manufacturing of metallic components, referred to as cold spray additive manufacturing (CSAM). Unlike the fusion-based AM processes, CSAM is achieved in a solid-state, bringing several advantages such as the absence of severe oxidation or phase composition changes. At the moment, the main limitation of CSAM is the generally low ductility of the as-sprayed deposits. In this paper, using Cu as a model material, we demonstrate a way to overcome this limitation. Importantly, a high ductility of the deposits in their as-sprayed state is achieved without a trade-off in mechanical strength. Furthermore, we show that without any post-heat treatment, the properties of CSAM Cu are comparable to bulk, non-AM Cu.

1. Introduction

Lately, cold spray technology (CS) is gradually recognized as a new additive manufacturing (AM) technique. In the cold spray process, micron-sized powder particles are accelerated by a propelling gas fed through a de Laval nozzle. The particles then impact onto the mandrel/substrate at supersonic velocities and undergo extensive plastic deformation, creating a firm bond with the underlying material [1–3]. Cold spray offers short production times, great process economy, virtually unlimited component size capability, and flexibility for a localized deposition. Given these, the CS process actually offers unique advantages over the AM techniques where thermal energy is the main principle of deposition (selective laser melting, electron beam melting, laser engineered net shaping and laser metal deposition) [4, 5]. Moreover, since the CSAM is done in a solid state, the production of metallic parts is without severe oxidation or phase changes [6, 7], and importantly, CS is more suited for AM of high reflectivity metals (such as Cu) that are problematic to process using the laser-assisted AM processes [8].

The cold spray process is now a well-established technique for metallic deposits in various industries. It has been used to produce protective or performance enhancing coatings, as well as near net shapes [9]. Aside from these, CS has also been proven to be a cost-effective process for repair and restoration of damaged aerospace components (in [10], a repair of Seahawk helicopter modules using CS is presented, leading to savings as high as 35–50% of a new component manufacture price).

At the moment, the main limitation of the cold spray process is the extremely low ductility of the deposits, an attribute arising from the severe plastic deformation of the powder particles and the associated cold work hardening phenomenon. To restore the ductility, CSAM materials are often subjected to a heat treatment to induce recrystallization and consolidation [11]. This high mechanical strength with almost zero ductility in the as-sprayed state and a subsequent ductility enhancement by post-heat treatment was reported by several researchers. For instance, Meng et al. [12] observed less than 1% elongation in the cold sprayed 304 stainless steel, which was enhanced 5× after heat treatment. In the case of Inconel 718, it has been observed that elongation in the as-sprayed material was only 0.5%, which increased 8–10x after annealing [13–15]. Yu et al. (2019) also observed the high mechanical strength and poor ductility with almost no elongation in the case of Cu, which, yet again, improved by heat treatment [16]. Yin et al. (2018) reported ~ 2.5% elongation in the as-sprayed state of cold sprayed Cu, which was improved by 7.6% after annealing at 500 °C for 4 h [17].

The presented study demonstrates a method to overcome this problem. Our Cu deposits exhibited high ductility in the as-sprayed state without any heat treatment. Importantly, this was achieved without any significant trade-off with regard to their mechanical strength and using

* Corresponding author.
E-mail address: rs@impact-innovations.com (R. Singh).

https://doi.org/10.1016/j.addlet.2022.100052
Received 15 March 2022; Received in revised form 2 May 2022; Accepted 2 May 2022

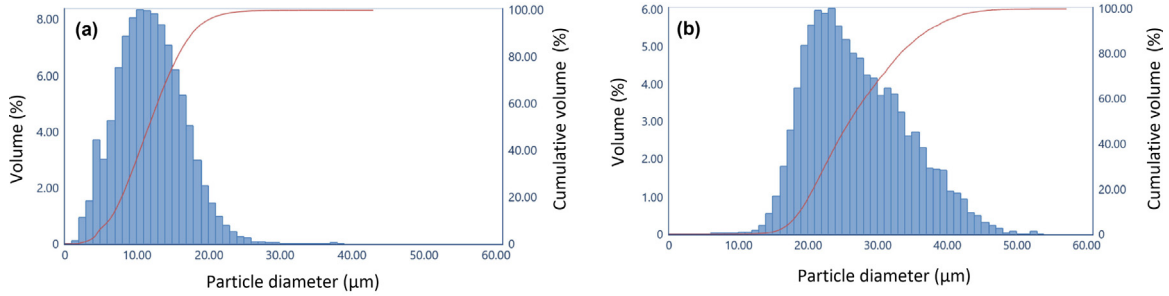

Fig. 1. Particle size distribution of the used (a) fine and (b) coarse Cu powders.

Table 1
Deposition process parameters.

Parameter	Fine-LP	Fine-HP	Coarse-LP	Coarse-HP
Process gas temperature (°C)	450	750	450	750
Process gas pressure (MPa)	3.8	5.0	3.8	5.0
Carrier gas flow (m^3/h)	4	4	4	4
Particle size distribution D_{50} (µm)	11.8	11.8	26.1	26.1
Powder deposition efficiency (%)	99	99	99	99

cheaper nitrogen as a process gas (no helium needed). In this paper, the influence of powder particle sizes and process parameters on microstructural and mechanical properties is presented, and the properties of our CSAM Cu in the as-sprayed state are further compared with bulk Cu.

2. Material and methods

2.1. Powder feedstock

Two high purity Cu powders (99.95%, Impact Innovations GmbH) with different particle size distributions were used to demonstrate the discovered principle (Fig. 1). The atomized powders had a spherical morphology, shown in Figure 22 for the fine powder with D_{10} = 6.2 µm, D_{50} = 11.8 µm, D_{90} = 17.8 µm and the coarse powder with D_{10} = 18.9 µm D_{50} = 26.1 µm, D_{90} = 40 µm.

2.2. Deposition process

Impact Innovations ISS 5/8 high-pressure gun with central injection system and OUT 1 nozzle (expansion ratio 5.6) was used for the deposition. Nitrogen was used as a propellant and feedstock carrier gas. Combining two feedstock powders (fine, coarse) and two proposed sets of process parameters (low - LP, high – HP, Table 1), four sample sets were prepared. The values of parameters for LP and HP were obtained in a preliminary in-house study. For all four depositions, a gun traverse speed of 500 mm/s, a stand-off distance of 30 mm, and a raster step size of 1 mm were used. The deposition parameters matrix is provided in Table 1. For each set, two aluminum plates of 70 × 70 mm^2 dimensions were used as substrates for deposition of 5–6 mm thick Cu coatings. After the deposition, the plates were removed to obtain free-standing Cu deposits. No additional heat treatment was performed.

To help understand the underlying principles, the in-flight velocity of the powder particles was measured by CSM EVOLUTION cold spray meter (Tecnar Automation Inc., Canada) equipped with a continuous diode laser source to illuminate the particle plume (790 nm wavelength, 3.3 W power, 70 mrad divergence).

2.3. Sample characterization

Metallographic samples were prepared from the deposits using standard procedures with the final polishing realized using a 1-µm diamond paste. The sample cross-sections were analyzed using EVO MA 15 scanning electron microscope (Carl Zeiss, Germany). The microstructural analysis was extended by advanced electron backscatter diffraction (EBSD) mapping using FEG/SEM Zeiss Ultra Plus (Carl Zeiss, Germany) equipped with HKL Nordlys EBSD detector (Oxford Instruments, UK). The EBSD data sets were acquired at an acceleration voltage of 20 kV with a 120 µm aperture in high/current mode using Aztech software (Oxford Instruments, UK). The acquisition step size was 200 nm, and the camera binning was adapted to reliable pattern recognition (4 × 4, in this case).

The compactness of the samples was assessed through a gas tightness test using a helium-leak detector (Qualytest HTL 260, Pfeiffer Vacuum GmbH, Asslar, Germany) in IEK-1, Forschungszentrum Jülich, Germany. A flow of He was maintained at one side of the deposits, while a vacuum was drawn on their other side. The amount of He leaking through the samples was recorded.

For mechanical properties testing, a tensile test and hardness measurement were selected. For the former, flat specimens (having a length of 60 mm) were EDM-cut out of the free-standing Cu deposits and the test was performed using a conventional tensile rig according to the EN ISO 6892–1 standard, except that the suggested mechanical extensometer was replaced with a virtual digital image correlation (DIC) extensometer. This setup has previously been assessed as an effective way for material characterization [18, 19] and it was shown that the contactless extensometer yields results fully comparable to those acquired by the mechanical extensometer. Using the virtual extensometer has another advantage, minimizing the probability of crack initiation due to sample surface scratching by the extensometer knife. A tensile load was applied at a constant rate of 0.4 mm/min until the fracture and the material's stress response was recorded. The hardness of the deposits was measured by the Vickers method using Q10A+ (Qness, Austria). Considering the grain sizes and microstructure features, a load of 300 gf was selected ($HV_{0.3}$) for all samples. The measurements were carried out following the ISO 6507–1 standard (spacing of indents at least 3× the indent size). Twenty indentations were used to calculate the average value of each sample. A two-tailed unpaired *t*-test was used to determine the statistical significance between hardness of deposits produced at LP and HP for both fine and coarse powders. The used level of significance was $^{*}p = 0.01$.

Thermal conductivity λ of the samples was calculated based on the measurements of thermal diffusivity a, density ρ, and heat capacity c_p according to the formula $\lambda = a \times \rho \times c_p$. The measurement of thermal diffusivity was performed by a laser flash method in a vacuum using the LFA 1000 tester (Linseis, Germany). To ensure uniform absorption

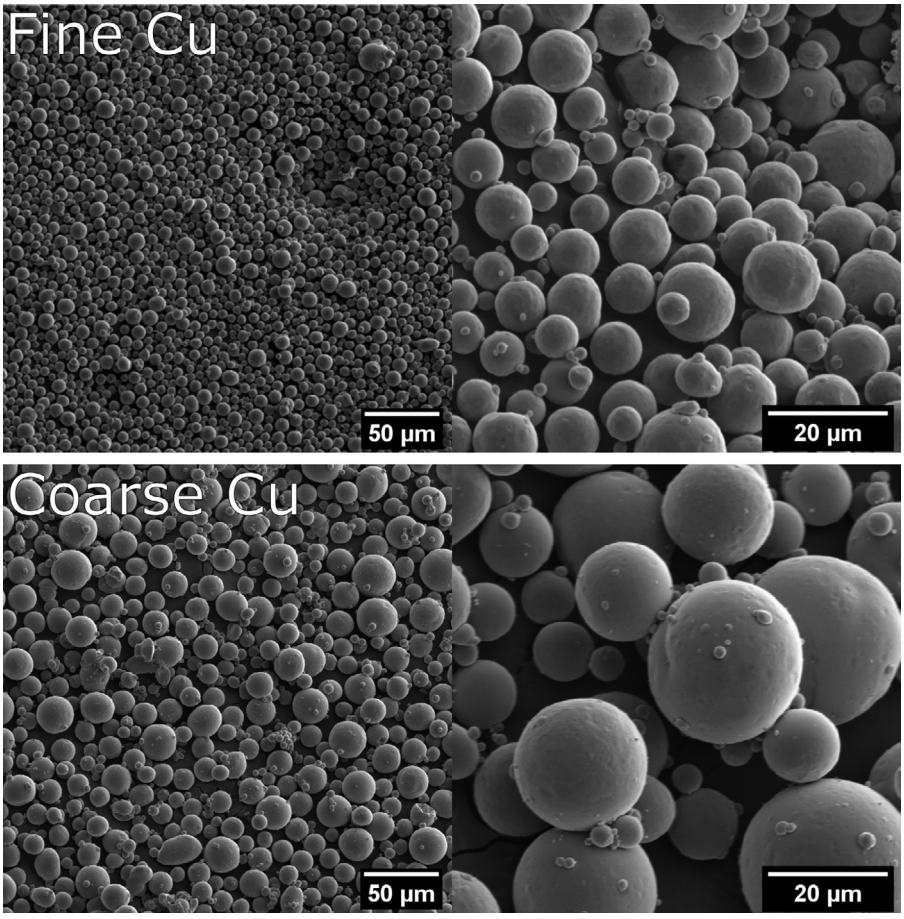

Fig. 2. Spherical morphology of the used fine and coarse Cu powders.

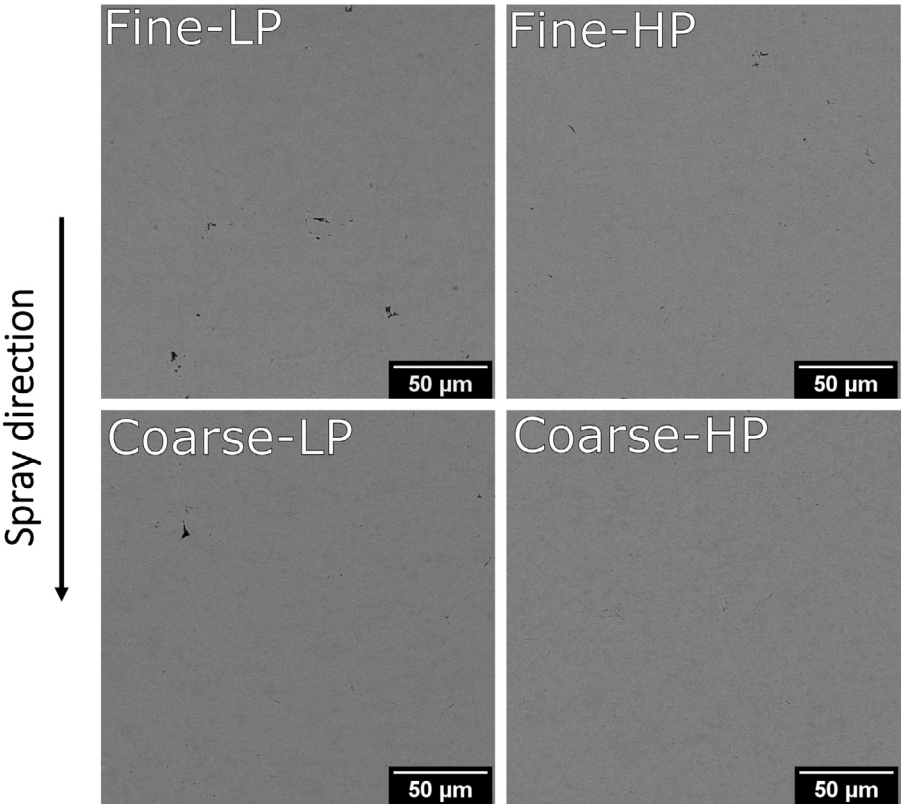

Fig. 3. Dense microstructure of the four CSAM Cu deposits.

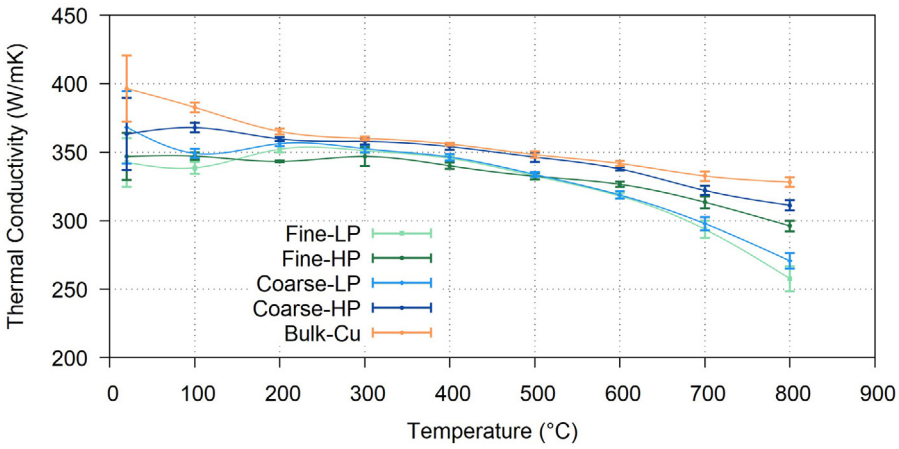

Fig. 4. Thermal conductivity of the four CSAM Cu deposits and bulk Cu.

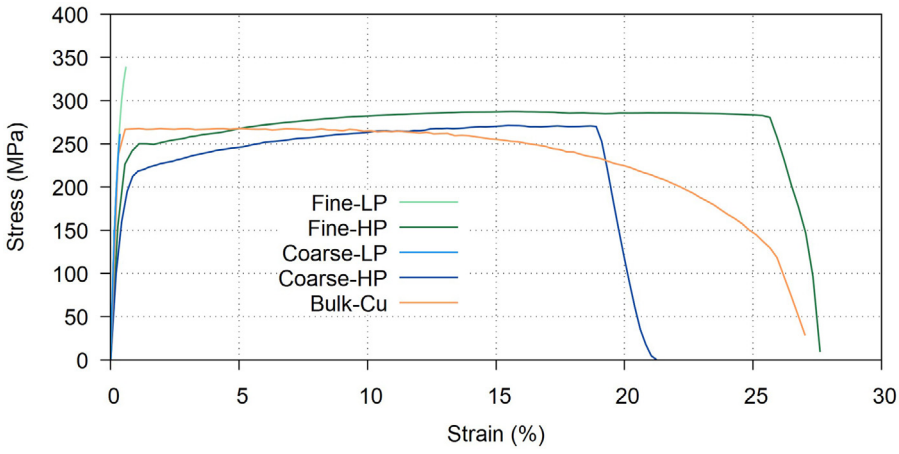

Fig. 5. Stress-strain curves showing high strength and ductility of cold sprayed Cu deposited at high process parameters, fully comparable to those of bulk Cu.

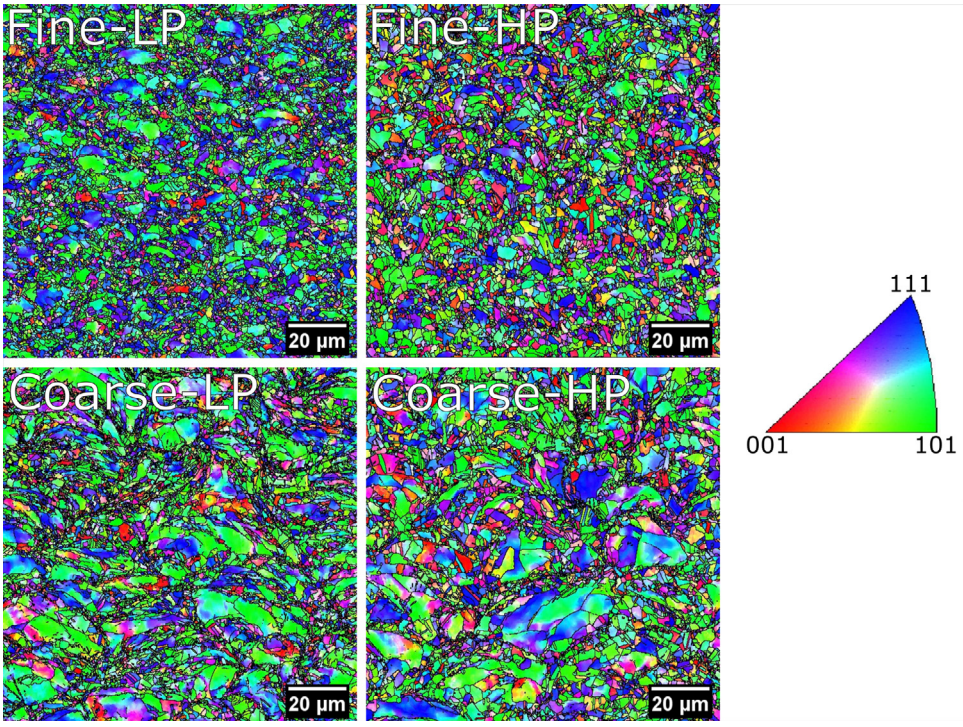

Fig. 6. EBSD IPF maps of the cold sprayed Cu deposits microstructure showing bimodal grain distribution.

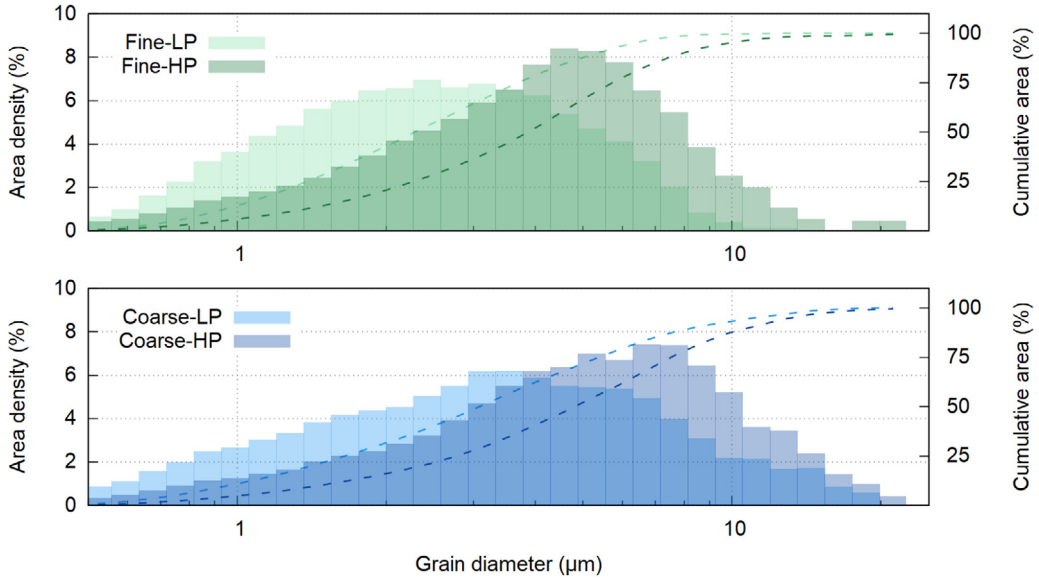

Fig. 7. Area grain size distribution in CSAM Cu deposits.

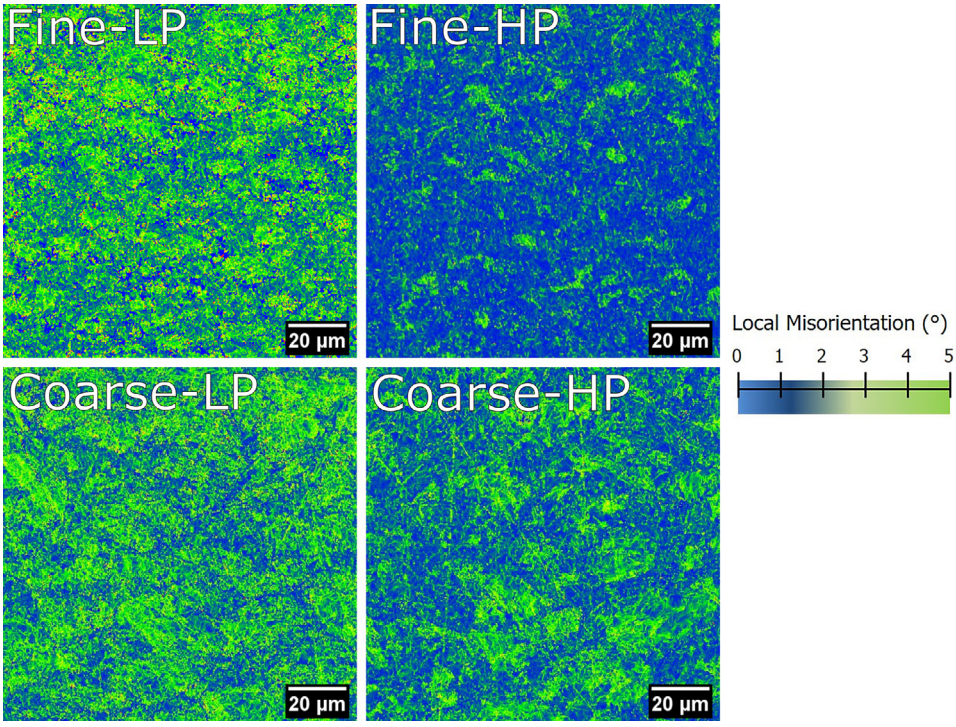

Fig. 8. Local grain misorientation maps of the cold sprayed Cu showing the amount of localized plastic strain.

of the laser pulse and equal radiation properties of the surfaces, the $10 \times 10 \times 2$ mm^3 samples were coated with a thin layer of graphite. For all samples, five measurements were taken at every temperature from 20 to 800 °C. The density ρ of the samples was measured using the Archimedes method (immersion of samples in water) and its respective temperature dependence was calculated based on the density temperature dependence of pure bulk Cu. For the calculations, the heat capacity c_p of pure copper was used.

The obtained properties measured by various methods were compared against bulk Cu material. To avoid incorporation of potential secondary influences and maintain a full mutual comparability, the Cu bulk was an identical material from which the two powders used here were atomized.

3. Results and discussion

3.1. Microstructure and thermal properties

The SEM BSE micrographs shown in Figure 33 demonstrate a very dense microstructure of the materials deposited from both powders at low and high parameters. In fact, the densities of Cu deposits determined by the Archimedean immersion method (Table 2) correspond to porosities lower than 1.5%, i.e., values comparable to bulk, metallurgical Cu. To assess the density further, a gas tightness test of the dense Cu deposits was carried out using He leak detection. In all deposits, a He flowrate smaller than 1×10^{-7} mbar•l/s was observed. According to [20, 21], the values below 1×10^{-7} mbar•l/s are considered a very

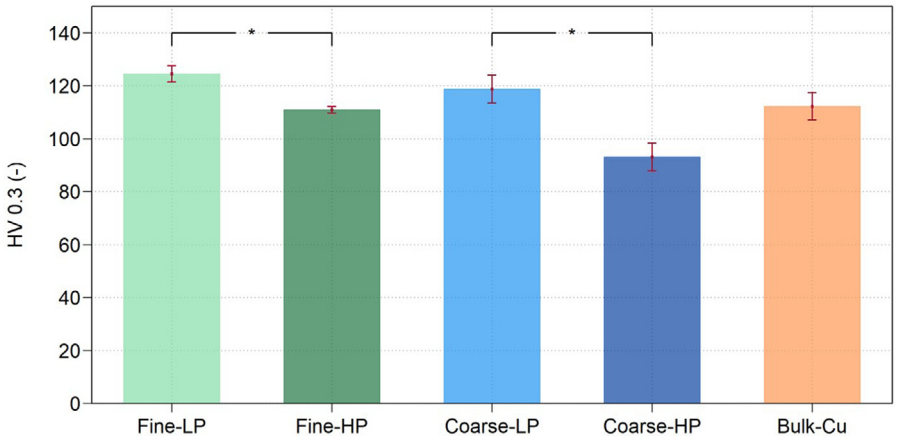

Fig. 9. Vickers $HV_{0.3}$ hardness of the four CSAM Cu deposits and bulk Cu. Asterisk denotes a significant statistical difference between the mean values at a confidence level of $p = 0.01$.

Table 2
Properties of cold sprayed Cu-deposits in comparison to bulk-Cu at room temperature.

Sample	Archimedes density (g/cm^3)	Thermal conductivity (W/m•K)	Yield strength (MPa)	Ultimate tensile strength (MPa)	Ductility (%)	Hardness ($HV_{0.3}$)
Fine-LP	8.79	342 ± 18	320 ± 6	326 ± 12	0.2 ± 0.1	125 ± 3
Fine-HP	8.84	346 ± 17	226 ± 3	286 ± 2	24.0 ± 2.8	111 ± 1
Coarse-LP	8.80	368 ± 26	245 ± 15	245 ± 15	0.1 ± 0.0	119 ± 5
Coarse-HP	8.81	363 ± 26	192 ± 8	268 ± 4	20.0 ± 0.4	93 ± 5
Bulk Cu	8.96	396 ± 24	272 ± 9	275 ± 9	26.0 ± 2.2	112 ± 5

tight system. In other words, the test confirmed that the cold sprayed deposits are very dense, and the limited porosity in the Cu-deposits is not interconnected.

The achieved density values stand out even more if compared against the Cu manufactured by other AM processes. For instance, Lykov et al. (2016) achieved 88.1% density in Cu produced by selective laser melting process [22], while Kumar et al. (2019) measured 77% to 97% density in sintered and HIPed Cu produced by binder jetting additive manufacturing [23].

Thermal conductivity of the Cu deposits was recorded in the temperature range of 20–800 ˚C, as shown in Fig. 4. It can be observed that the thermal conductivity of all samples is comparable to the bulk Cu counterpart, indirectly confirming the deposits quality. The slightly better values of both HP deposits (pronounced at higher temperatures) likely stem from their slightly better density and different microstructure topology (discussed in Section 3.2.1). It can also be observed that the coarse powder deposits demonstrated a slightly higher thermal conductivity than the finer powder deposits, a trend similar at both process parameters. This could, again, be caused by the specific microstructure topology. For all samples, the thermal conductivity decreases with increasing temperature. In metals, this is a well-known phenomenon as their thermal conductivity mostly depends on the flow of electrons, which is hindered by lattice vibrations at increased temperatures [24, 25].

3.2. Mechanical properties

3.2.1. Tensile strength and ductility

The representative stress-strain curves are shown in Fig. 5. These results show that at LP, both cold sprayed deposits exhibit a high tensile strength accompanied by a very low ductility. Such properties are typical for the as-deposited CSAM materials and are a consequence of the extreme work hardening during the plastic deformation of the powder particles. The game-changing results are the curves obtained for Cu samples deposited at HP. These are characterized by high tensile strength as well as high ductility, both fully comparable to the bulk (i.e., non-AM) counterpart. Developing an AM material with a simultaneous high strength and high ductility has always been a challenging task, in particular since strength and ductility are usually mutually exclusive. To the best of our knowledge, such a result for cold sprayed Cu in the as-sprayed state has not been reported previously.

The tensile test data further suggest that the Cu deposits sprayed at both process parameters using the finer powder show higher strength when compared to their counterparts sprayed from the coarser feedstock. This effect is, however, less significant than the influence of the process parameters.

Grain refinement from coarse grains down to ultrafine and further to nanoscale grains is a well-known approach to strengthen metallic materials [26,27]. The penalty in this approach is usually a poor ductility due to the limited capacity to store dislocations that results in an early strain localization during mechanical loading. To overcome this, fabrication of bimodal grain size microstructure has been proven as a strategy to enhance the ductility in ultrafine grain materials, at a little sacrifice in tensile strength. In materials with such bimodal grain size distribution, the ultrafine grains provide high strength, whereas the coarse grains work as sinks for dislocations storage and enhance the ductility [28–31]. The tensile test data suggested that at HP, the Cu deposits could possess such bimodal microstructure, providing them with high strength and ductility. To investigate this hypothesis and also to detect the potential microstructure recrystallization, EBSD inverse pole figures (IPF) and local grain misorientation (KAM) maps of all four CSAM deposits were acquired.

The IPF maps presented in Figure 66 clearly show a specific microstructure where coarse grain areas located in the center of the original Cu particles are enclosed in a continuous network of few micrometer-sized ultra-fine grains along the particles' rims. The IPF maps of Fine-LP (particle velocity 688 m/s) and Fine-HP (particle velocity 813 m/s) deposits show a clearly visible bimodal structure formed at both process parameters. However, at LP, the spatial topological distribution of the coarse grains and fine grains is not homogenous, with some areas showing only the fine grains, and the ultrafine grains network is further not homogeneously distributed. Contrary to LP, the microstructure of the Fine-HP deposits demonstrates a homogeneous spatial topological distribution of the coarse and the fine grains, with coarse grain areas

regularly surrounded by the interconnected ultrafine grains network. As discovered in other studies (e.g., Zhang et al. for 304 L stainless steel [32]), the spatial topological distribution (discussed for our deposits) is another factor that plays a major role in achieving the simultaneous high ductility and high strength at HP. A similar behavior was observed in the microstructure of the coarse Cu powder deposits at LP and HP: the microstructure of Coarse-LP (particle velocity 591 m/s) illustrates a non-homogeneously distributed elongated big grains, along with irregular and relatively thicker ultrafine grains network, while Coarse-HP (particle velocity 662 m/s) shows more homogeneously distributed coarse grain areas surrounded by relatively thinner ultrafine grain walls. In all deposits the elongated coarse grains observed in the microstructure could appear because of the jetting phenomenon during the powder particle impact, as also reported by Borchers et al. [33] and Rahmati et al. [34].

From the EBSD results, it is clear that all four deposits exhibit a bimodal structure, but they differ in the ratio of fine and coarse grains. To quantify the difference, the EBSD IPF maps were used to calculate the area-weighted grain size distribution within each deposit (Fig. 7). The histograms clearly show that the process parameters (LP vs. HP) significantly influence the grain size distribution. For both types of feedstock powder, the deposits sprayed at HP show a higher proportion of larger grains. Such shift is triggered by the discussed grain recrystallization and gives rise to a microstructure composed of fine and coarse grains alike. In terms of absolute values, the median grain sizes shifted from 2.3 μm to 3.9 μm and from 3.1 μm to 4.8 μm for the fine and the coarse powders, respectively. Furthermore, unlike the influence of process parameters, there is no significant difference between the two powders under LP and HP.

To further understand the microstructure formation, local grain misorientation (KAM) maps were calculated from the IPF maps, revealing the amount of plastic strain in the deposits (Fig. 8). The results suggest that both deposits sprayed at LP exhibit a highly strained interior of the coarse grains as well as the grain boundaries. It can also be observed that the proportion of non-indexed area (mostly limited to particle boundaries and at the coarse-fine grains interface regions) is higher in the Fine-LP, indicating either a highly deformed region with high dislocation density or very small nanocrystalline features below the EBSD resolution limits. The misorientation maps of both HP deposits show a less strained area and almost no non-indexed area compared to the maps of LP.

Combined, the EBSD results indicate that although the plastic strain still exists, thermal softening and recrystallization were dominating the shear straining caused by the very high particle impact velocities. It has also been reported in the literature that in the case of copper, particle velocities exceeding 600 m/s are sufficient to increase the localized temperature close to the melting point, i.e., high enough for a dynamic recrystallization in the highly strained material [33–35]. The particle velocities achieved in our study at both LP and HP are sufficient to trigger this process for both powders.

In the previous studies {e.g., [33]}, it has been proposed that microstructure evolution during a dynamic recrystallization for high strain rate deformation occurs in five stages: (i) random distribution of dislocations, (ii) dynamic recovery by the formation of elongated dislocation cells, (iii) elongated dislocation cells arrangement to form elongated sub-grains, (iv) break-up of the elongated sub-grains, and (v) formation of recrystallized microstructure with small equiaxed grains. As also reported by Borchers et al. (2003) and Schmidt et al. (2006), a higher particle velocity produces a higher localized temperature rise, which then provides more time for the microstructure evolution [33, 36].

The results presented in the current study suggest that at LP, the elevated temperature conditions exist for an insufficient amount of time only, and, therefore, the recrystallization cannot fully evolve. Instead, the microstructure development ceases at the early stage, and, as a result, the observed highly strained and heterogeneous bimodal microstructure is formed. This affects the mechanical properties of the CSAM Cu deposits, displaying the high strength but very low ductility. Contrary to this, at HP, the higher particle velocities of both powders induce higher temperatures, thereby facilitating dynamic recrystallization and stimulating a fully evolved bimodal microstructure with relaxed grains. The results further indicate a homogenous and relaxed bimodal microstructure where the coarse grain areas are surrounded by a continuous network of ultrafine grains is required to obtain the synergistic effect of simultaneous high strength and high ductility. In our study, this was observed for both powders sprayed at HP. The bimodal microstructure in the cold sprayed Cu was also reported earlier by Jakupi et al. (2015) [35]. However, the bimodal structures presented there showed heterogeneity in the spatial topological distribution of both the coarse grain areas and the ultrafine grains network, and, as a result, the observed high strength was accompanied by a very low ductility, similar to our results at LP.

Fig. 2–6

3.2.2. Hardness

Fig. 9 demonstrates the influence of the powder particle size and the process parameters on hardness of the CSAM Cu deposits. The hardness follows the trend observed for the tensile strength behavior (Fig. 5), i.e., the fine powder deposits show higher values due to their finer grain structure (shown in Figure 66). The fine-grain microstructure contains a high density of grain boundaries, which act as obstacles for dislocation motion, resulting in dislocations pileups in the regions close to the grain boundaries during the indentation. Consequently, a higher stress is required to move the dislocations through these pileups, resulting in an increase in hardness [37].

At the used process parameters, the difference in the hardness values of the fine and coarse powder deposits is not very significant, though. As opposed to this, the effect of the process parameters is manifested nicely. The statistical analysis by a two-tailed *t*-test indicates a significant difference between the mean values ($p < 0.01$) of hardnesses of the samples deposited at LP and HP. Apparently, as discussed in Section 3.2.1, at LP, the shear straining dominates over recrystallization, while at HP, a fully recrystallized and relaxed microstructure was obtained. As a result, the hardness decreases for both HP deposits. The very low standard deviations suggest that all four CSAM Cu deposits are very homogenous in terms of their macro-properties. Last, the cold sprayed Cu deposits have a hardness comparable to bulk Cu.

4. Conclusions

Pure copper CSAM deposits have been produced using spherical powders, a high-pressure gun, and nitrogen as a process gas. The influence of process parameters and powder particle size has been investigated. From the results, the following conclusions can be drawn:

- Almost pore-less Cu deposits (density of 8.79–8.84 g/cm3, fully suppressing helium leak) can be produced by CSAM, having a high thermal conductivity of 368 W/m•K comparable to bulk Cu (396 W/m•K) in their as-sprayed state.
- Without any secondary processing (such as heat treatment), a simultaneous high strength and high ductility can be achieved in the deposits at high spray parameters, regardless of the used Cu powder. This is provided by the favorable topology of the bimodal microstructure, consisting of coarse grains enclosed in a network of fine grains along the individual particle rims.
- The process gas parameters (temperature and pressure) have a more significant influence on the mechanical properties than the used feedstock average particle size. A combination of the ultimate tensile strength of 286 MPa and 24% ductility was achieved in CSAM Cu.

The thermo-mechanical properties of the CSAM Cu deposits developed in our work are fully comparable to bulk Cu produced by a non-additive metallurgy method. Considering the high deposition efficiency (99%) and high deposition rates, this letter illustrates a huge potential

of the method to be implemented in various industrial sectors for either demanding applications or even in serial production.

Declaration of competing interests

The authors declare that they have no known competing financial interests or personal relationships that could have appeared to influence the work reported in this paper.

Acknowledgements

Authors greatly acknowledge Mr. Stefan Heinz, Dr. Georg Mauer, and Dr. Stefan Baumann, Institute of Energy and Climate Research, Material Synthesis and Processing (IEK-1), Forschungszentrum Jülich, Germany, for performing the He-leak tests in the cold sprayed copper samples. Authors would also like to thank Mr. Lukas Loidl for his support in cold spraying and Mr. Maximilian Meinicke's support in project management. This work was funded by Impact Innovations GmbH, Germany. Part of the sample characterization was funded by COMTES FHT a.s. within the project "Pre-Application Research of Functionally Graduated Materials by Additive Technologies, No. CZ.02.1.01/0.0/0.0/17_048/0007350, financed from European Regional Development Fund" and by the Institute of Plasma Physics of the Czech Academy of Sciences with the Czech Science Foundation project 22-14048S.

References

[1] A. Papyrin, V. Kosarev, S. Klinkov, A. Alkhimov, V.M. Fomin, Cold spray technology, Cold Spray Technol (2007), doi:10.1016/B978-0-08-045155-8.X5000-5.
[2] V.F. Kosarev, S.V. Klinkov, A.P. Alkhimov, A.N. Papyrin, On some aspects of gas dynamics of the cold spray process, J. Therm. Spray Technol. 12 (2003) 265–281, doi:10.1361/105996303770348384.
[3] M. Grujicic, C.L. Zhao, C. Tong, W.S. DeRosset, D. Helfritch, Analysis of the impact velocity of powder particles in the cold-gas dynamic-spray process, Mater. Sci. Eng. A. 368 (2004) 222–230, doi:10.1016/j.msea.2003.10.312.
[4] C. Lee, J. Kim, Microstructure of kinetic spray coatings: a review, J. Therm. Spray Technol. 24 (2015) 592–610, doi:10.1007/S11666-015-0223-5/FIGURES/3.
[5] X.T. Luo, C.X. Li, F.L. Shang, G.J. Yang, Y.Y. Wang, C.J. Li, High velocity impact induced microstructure evolution during deposition of cold spray coatings: a review, Surf. Coatings Technol. 254 (2014) 11–20, doi:10.1016/J.SURFCOAT.2014.06.006.
[6] T. Schmidt, H. Assadi, F. Gärtner, H. Richter, T. Stoltenhoff, H. Kreye, T. Klassen, From particle acceleration to impact and bonding in cold spraying, J. Therm. Spray Technol. 18 (2009) 794–808, doi:10.1007/S11666-009-9357-7/FIGURES/22.
[7] J. Pattison, S. Celotto, R. Morgan, M. Bray, W. O'Neill, Cold gas dynamic manufacturing: a non-thermal approach to freeform fabrication, Int. J. Mach. Tools Manuf. 47 (2007) 627–634, doi:10.1016/J.IJMACHTOOLS.2006.05.001.
[8] Q. Jiang, P. Zhang, Z. Yu, H. Shi, D. Wu, Xin Ye H.Yan, Q. Lu, Y. Tian, A review on additive manufacturing of pure copper, Coatings 11 (2021) 740, doi:10.3390/coatings11060740.
[9] J. Karthikeyan, in: Cold Spray Technology: International Status and USA Efforts, ASB industries Inc., 2004, pp. 1–14. http://www.asbindustries.com/documents/int_status_report.pdf.
[10] N. Matthews, Cold Spray in Australian Aerospace Industries, TSS Cold Spray Conf., Akron, Ohio, USA, 27-29 September, 2010.
[11] J. Villafuerte, Modern Cold Spray : Materials, Process, and Applications, Springer International Publishing, Cham, Switzerland, 2015, doi:10.1007/978-3-319-16772-5.
[12] X.M. Meng, J.B. Zhang, W. Han, J. Zhao, Y.L. Liang, Influence of annealing treatment on the microstructure and mechanical performance of cold sprayed 304 stainless steel coating, Appl. Surf. Sci. 258 (2011) 700–704, doi:10.1016/J.APSUSC.2011.07.107.
[13] W. Ma, Y. Xie, C. Chen, H. Fukanuma, J. Wang, Z. Ren, R. Huang, Microstructural and mechanical properties of high-performance Inconel 718 alloy by cold spraying, J. Alloys Compd. 792 (2019) 456–467, doi:10.1016/j.jallcom.2019.04.045.
[14] W. Wong, E. Irissou, P. Vo, M. Sone, F. Bernier, J.G. Legoux, H. Fukanuma, S. Yue, Cold spray forming of Inconel 718, J. Therm. Spray Technol. 22 (2013) 413–421, doi:10.1007/S11666-012-9827-1/FIGURES/10.
[15] S. Bagherifard, G. Roscioli, M.V. Zuccoli, M. Hadi, G. D'Elia, A.G. Demir, B. Previtali, J. Kondás, M. Guagliano, Cold spray deposition of freestanding inconel samples and comparative analysis with selective laser melting, J. Therm. Spray Technol. 26 (2017) 1517–1526, doi:10.1007/S11666-017-0572-3.
[16] B. Yu, J. Tam, W. Li, H.J. Cho, J.-.G. Legoux, D. Poirier, J.D. Giallonardo, U. Erb, Microstructural and bulk properties evolution of cold-sprayed copper coatings after low temperature annealing, Materialia 7 (2019) 100356, doi:10.1016/j.mtla.2019.100356.
[17] S. Yin, R. Jenkins, X. Yan, R. Lupoia, Microstructure and mechanical anisotropy of additively manufactured cold spray copper deposits, Mater. Sci. Eng. A 734 (2018) 67–76, doi:10.1016/j.scriptamat.2017.09.042.
[18] R. Procházka, P. Sláma, J. Dlouhý, P. Konopík, Z. Trojanová, Local mechanical properties and microstructure of EN AW 6082 aluminium alloy processed via ECAP–conform technique, Materials 13 (2020) 2572, doi:10.3390/MA13112572.
[19] J. Džugan, M. Sibr, P. Konopík, R. Procházka, M. Rund, Mechanical properties determination of AM components, IOP Conf. Ser. Mater. Sci. Eng. (2017) 179, doi:10.1088/1757-899X/179/1/012019.
[20] H. Rottländer, W. Urath, G. Voss, Fundamentals of leak detection, Ed. Leybold GmbH, Cat. No. 199 79_VA.02. https://pdf.directindustry.com/pdf/leybold/fundamentals-leak-detection/13869834481.html. (Accessed 12th December 2016).
[21] Leak Detection Compendium, Ed. Pfeiffer Vacuum GmbH, https://leak-detection.pfeiffer-vacuum.com/en/leak-detection-know-how/. (Accessed April 2013).
[22] P.A. Lykov, E.V. Safonov, A.M. Akhmedianov, Selective laser melting of copper, Mater. Sci. Forum 843 (2016) 284–288, doi:10.4028/www.scientific.net/MSF.843.284.
[23] A.Y. Kumar, J. Wang, Y. Bai, S.T. Huxtable, C.B. Williams, Impacts of process-induced porosity on material properties of copper made by binder jetting additive manufacturing, Mater. Des. 182 (2019) 108001, doi:10.1016/J.MATDES.2019.108001.
[24] S. Aksöz, E. Öztürk, N. Maraşlı, The measurement of thermal conductivity variation with temperature for solid materials, Measurement 46 (2013) 161–170, doi:10.1016/j.measurement.2012.06.003.
[25] Z. Tong, S. Li, X. Ruan, H. Bao, Comprehensive first-principles analysis of phonon thermal conductivity and electron-phonon coupling in different metals, Phys. Rev. B 100 (2019) 144306, doi:10.1103/PhysRevB.100.144306.
[26] R. Valiev, Materials science: nanomaterial advantage, Nature 419 (2002) 887–889, doi:10.1038/419887A.
[27] T.G. Langdon, Twenty-five years of ultrafine-grained materials: achieving exceptional properties through grain refinement, Acta Mater 61 (2013) 7035–7059, doi:10.1016/j.actamat.2013.08.018.
[28] M.A. Meyers, A. Mishra, D.J. Benson, Mechanical properties of nanocrystalline materials, Prog. Mater. Sci. 51 (2006) 427–556.
[29] Y. Estrin, A. Vinogradov, Extreme grain refinement by severe plastic deformation: a wealth of challenging science, Acta Mater 61 (2013) 782–817, doi:10.1016/J.ACTAMAT.2012.10.038.
[30] X. Li, K. Lu, Refining grains of metals through plastic deformation: toward grain size limits, Acc. Mater. Res. 2 (2021) 108–113, doi:10.1021/accountsmr.0c00075.
[31] C.C. Koch, Optimization of strength and ductility in nanocrystalline and ultrafine grained metals, Scr. Mater. 49 (2003) 657–662, doi:10.1016/S1359-6462(03)00394-4.
[32] Z. Zhang, D. Orlov, S. Kumar Vajpai, B. Tong, K. Ameyama, Importance of Bimodal Structure Topology in the Control of Mechanical Properties of a Stainless Steel, Adv. Eng. Mater. 17 (2015) 791–795, doi:10.1002/adem.201400358.
[33] C. Borchers, F. Gärtner, T. Stoltenhoff, H. Assadi, H. Kreye, Microstructural and macroscopic properties of cold sprayed copper coatings, J. Appl. Phys. 93 (2003) 10064, doi:10.1063/1.1573740.
[34] S. Rahmati, A. Zúñiga, B. Jodoin, R.G.A. Veiga, Deformation of copper particles upon impact: a molecular dynamics study of cold spray, Comp. Mat. Sci. 171 (2020) 109219–110927, doi:10.1016/j.commatsci.2019.109219.
[35] P. Jakupi, P.G. Keech, I. Barker, S. Ramamurthy, R.L. Jacklin, D.W. Shoesmith, D.E. Moser, Characterization of commercially cold sprayed copper coatings and determination of the effects of impacting copper powder velocities, J. Nucl. Mater 466 (2015) 1–11, doi:10.1016/j.jnucmat.2015.07.001.
[36] T. Schmidt, F. Gärtner, H. Assadi, H. Kreye, Development of a generalized parameter window for cold spray deposition, Acta Mater 54 (2006) 729–742, doi:10.1016/J.ACTAMAT.2005.10.005.
[37] B.B. Jung, H.K. Lee, H.C. Park, Effect of grain size on the indentation hardness for polycrystalline materials by the modified strain gradient theory, Int. J. Solids Struct 50 (2013) 2719–2724, doi:10.1016/J.IJSOLSTR.2013.05.002.